Energy Conversion and Management: X 30 (2026) 101865

Contents lists available at ScienceDirect

Energy Conversion and Management: X

journal homepage: www.sciencedirect.com/journal/energy-conversion-and-management-x

A novel parallel solver using decoupled chemical–physical integration for rapid multizone simulation of reactivity controlled combustion in engines

Mohammad Mahdi Salahi [a,*], Jamshid Moradi [a], Kian Golbaghi [b], Shadab Heidarabadi [b], Amin Andwari [a,*], Jari Hyvönen [c], Maciej Mikulski [b]

[a] Machine and Vehicle Design (MVD), Materials and Mechanical Engineering, Faculty of Technology, University of Oulu, Oulu FI-90014, Finland
[b] Efficient Powertrain Solutions (EPS), School of Technology and Innovation, University of Vaasa, Wolffintie 34, Vaasa FI-65200, Finland
[c] Wärtsilä Finland OY, Järvikatu 2-4, Vaasa 65101, Finland

ARTICLE INFO

Keywords:
Multizone model
RCCI engine
Acceleration
Parallel processing
Chemical mechanism

ABSTRACT

This study presents a novel acceleration strategy for the University of Vaasa Advanced Thermo-kinetic multi-Zone (UVATZ) RCCI combustion model. The method decouples stiff chemical kinetics from interzonal physical transport processes using an implicit–explicit integration strategy, where chemical reactions are solved implicitly while transport phenomena are handled explicitly. This approach reduces the size of the Jacobian matrix, enables zone-wise parallelization, and allows tailored numerical solvers for different equation classes. The solver is implemented in C++ using the Cantera framework and validated using three operating points from a Wärtsilä W31DF dual-fuel marine engine. For a 13-zone configuration using a 54-species/269-reaction kinetic mechanism, the accelerated solver achieves 14.7–19.3 × speed-up compared to the baseline implicit solver while maintaining excellent agreement in combustion predictions. Key engine indicators including peak pressure, IMEP, CA10, CA50, and net heat release remain within 1.5% deviation from the baseline results. With a larger mechanism containing 143 species and 746 reactions, the acceleration increases to approximately 24 × . Furthermore, the proposed method exhibits near-linear runtime scaling with the number of zones, in contrast to the cubic scaling behavior of the baseline solver. For a 40-zone configuration, the method achieves up to 249 × reduction in runtime, enabling high-resolution multizone simulations that would otherwise be computationally impractical. The proposed framework substantially improves the computational efficiency of detailed RCCI multizone simulations while preserving predictive accuracy. This capability enables large parametric studies, transient engine cycle simulations, and model-based design applications for advanced low-emission marine engines.

Introduction

Despite the long-term transition toward carbon neutrality, combustion engines remain indispensable in high-power-density applications such as marine transport, where long range, fuel energy density, reliability, and operational flexibility are essential. Accordingly, the International Maritime Organization (IMO) envisages a gradual transition toward low-emission and low-carbon shipping, rather than the abrupt replacement of combustion-based propulsion systems [1]. This context has intensified research on sustainable fuels, advanced combustion concepts, and control strategies that can reduce environmental impact while preserving engine efficiency and load-following capability [2,3].

Within this transition, the central technical challenge is to reduce engine-out emissions, particularly NOx and soot, without compromising efficiency, combustion stability, or fuel flexibility. Low-temperature combustion (LTC) addresses this challenge by suppressing the high local temperatures that promote NOx formation and the locally rich regions that favor soot production [4]. Among LTC concepts, reactivity-controlled compression ignition (RCCI) has emerged as one of the most promising because it combines low-temperature heat release with a dual-fuel strategy [5–7]. In RCCI, a low-reactivity fuel (LRF), such as gasoline [8], alcohols [9,10], or methane [11,12], is premixed with air, while a high-reactivity fuel (HRF), typically biodiesel, or mineral diesel [11,13], is directly injected to trigger auto-ignition. This reactivity stratification enables strong control over combustion phasing and can substantially reduce NOx and soot. However, RCCI also introduces important challenges related to incomplete oxidation, pressure-rise-rate

* Corresponding authors.
E-mail addresses: Mahdi.Salahi@oulu.fi (M.M. Salahi), Amin.M.Andwari@oulu.fi (A. Andwari).

https://doi.org/10.1016/j.ecmx.2026.101865
Received 9 February 2026; Received in revised form 14 April 2026; Accepted 14 April 2026
Available online 16 April 2026

Nomenclature

Symbel	Definition
A	Surface area
ρ	Density
Q	Heat
ħ	Specific enthalpy
h	Heat transfer coefficient
k	Turbulent kinetic energy
D	Interzonal species transfer coefficient
Y	Mass fraction of species
X	Molar concentration of species
m	Mass
W	Molar mass
$\dot{\omega}$	Molar production rate of species
P	Pressure
T	Temperature
nZ	Total number of zones
Ru	Universal gas constant
L	Cylinder volume height
e	Specific energy
E	Internal energy
υ	Stoichiometric coefficients
g	Reaction rate
r	Radius
Λ	Conduction coefficient
V	Volume
$c_{v,p}$	Specific heat capacity

Abbreviations	Definition
AGI	Adaptive Grid Integration
AMECS	Advanced Model for Engine Combustion Simulation
BDF	Backward Differentiation Formula
CAD	Crank Angle Degree
CFD	Computational Fluid Dynamics
HCCI	Homogeneous Charge Compression Ignition
IMEP	Indicated Mean Effective Pressure
LTC	Low Temperature Combustion
LRF	low-reactivity fuel
MBD	Model-based design
MZM	Multi-Zone Model
NHR	Net Heat Release
ODE	Ordinary Differential Equation
RCCI	Reactivity Controlled Compression Ignition
RMS	Root Mean Square
UVATZ	University of Vaasa Advanced Thermo-kinetic multi-Zone
VVA	Variable Valve Actuation

Subscripts	**Definition**
cyl	Cylinder
z	Index for zones
i	Index of species
j	Index of reactions

control, and emissions of CO, unburned hydrocarbons, and methane slip, especially under dilute and low-load conditions [14,15]. Therefore, predictive tools are required to exploit RCCI benefits while managing its emissions trade-offs [16–18].

Although RCCI is governed by auto-ignition kinetics, it offers several interacting control levers, including the LRF/HRF ratio, HRF injection timing, in-cylinder reactivity stratification, and, more recently, variable valve actuation (VVA)-enabled thermal management 1917. As a result, RCCI calibration involves a large and strongly coupled parameter space 2021. Comprehensive experimental campaigns are therefore costly, time-consuming, and typically restricted to safe and near-steady operating regions. High-fidelity CFD can provide detailed spatial and temporal information, but its computational cost makes it unsuitable for broad parametric sweeps, control development, or rapid optimization [22].

For this reason, reduced-order physics-based models are essential in RCCI research. Model-based design (MBD) provides a virtual development environment in which engine concepts can be assessed before extensive hardware testing. Although such models require calibration, they enable rapid exploration of design and operating spaces and substantially reduce development time and cost. In RCCI applications, MBD models are especially attractive because they can maintain sufficient fidelity for predicting combustion phasing, performance, and emissions while remaining computationally tractable for iterative studies [16].

Among reduced-order combustion models, stochastic reactor models (SRMs) and multizone models (MZMs) are the two most relevant families for LTC and RCCI simulation. SRMs represent mixture inhomogeneity statistically through probability density function approaches and have shown good capability in describing LTC combustion phenomena [23,24]. However, for control-oriented studies and broad design exploration, MZMs remain particularly attractive because they preserve detailed chemistry at much lower cost than CFD and with a simpler structure than SRMs [25,26]. In an MZM, the cylinder is discretized into multiple coupled homogeneous reactors that exchange heat and mass while sharing a common pressure. This framework is well-suited to predicting heat release, combustion phasing, and the main exhaust-emission trade-offs of RCCI, including the simultaneous reduction of NOx and soot together with possible increases in CO, unburned hydrocarbons, and methane slip, without resolving full three-dimensional flow fields.

Table 1
Evolutionary trend of UVATZ model (Mikulski et al. [36]).

	UVATZ-MZ 1.0	**UVATZ-MZ 2.0/ GT-UVATZ**	**UVATZ-MZ 3.0**
Platform	C++ source code Cantera 2.5 0D libraries Robust solver CVODES	UVATZ 1.0 + GT-Power user code + modified Cantera flow objects	UVATZ 2.0 + GT-power combustion object + modified Cantera Reactors
Thermal and fuel stratification	13 onion zones Diffusion-based interzonal mixing Homogeneous conductivity Imposed fuel distribution	12 zones (10 cylindrical + 2 disk-shaped) + Spatial-dependent heat and mass transfer	12 zones (10 cylindrical + 2 disk-shaped) + CFD-calibrated fuel distribution model
Sub-models	Wall heat loss: Chang et al. Kinetics mech.: Yao et al.	+ Improved turbulence: Yang and Martin	+ Improved Turbulence: Energy cascade +Improved mechanism: Yao et al. + NOx
Advantages over earlier	Simulation time < 4 min Numerical stability Simple and fast	+ Integration with GT-power gas exchange model + Full-cycle analysis	+ Emission calibration + Multi-cylinder simulation + Integration with optimizer
Validated on	Wartsila 31 SCRE/ RCCI	Wartsila 31 SCRE/ RCCI	Wartsila 6 L20/ RCCI
Primary References	Vasudev et al. (2022)	Kakoee et al. (2023)	Vasudev, et al. (2024).
Applied in	Modabberian et al. (2023)Storm et al. (2023)	Kakoee et al. (2024) Modabberian et al. (2024)	Vasudev, et al. (2025)

Kodavasal et al. [27] classified multizone models into two main categories: balloon-type and onion-skin configurations. For RCCI applications, onion-skin formulations have become especially influential because they can represent thermal and compositional stratification in a computationally efficient manner. Egüz et al. [28], for example, used a 10-zone model with detailed kinetics to study the effects of injection timing and charge composition in a dual-fuel RCCI engine. Using fuel distributions informed by preliminary 3D simulations, their model reproduced ignition timing and heat-release behavior with good accuracy. Subsequent studies extended this framework toward diesel–natural gas RCCI, including spray-informed predictive zero-dimensional models [29,30], empirical heat-release formulations [31], and control-oriented multizone implementations with inter-zonal mixing and NOx submodels [32,33].

A particularly important development path is represented by the University of Vaasa Advanced Thermo-kinetic multi-Zone (UVATZ) framework, which targets large-bore marine RCCI engines. UVATZ is a quasi-dimensional model in which the HRF injection process is decoupled from combustion, and the resulting stratification is prescribed through a spray-trained submodel, while the LRF is introduced as a premixed charge. Across successive generations, UVATZ has evolved from a 13-zone onion-skin architecture toward more predictive formulations incorporating spatially dependent heat and mass transfer, boundary zones, GT-Power coupling for gas exchange, CFD-calibrated fuel-distribution models, and improved turbulence and emissions submodels [34,35]. As summarized in Table 1, these developments have improved both predictivity and applicability, and the third-generation model has been validated on the Wärtsilä W20 RCCI platform [2]. Despite these advances, the computational burden of detailed multizone models remains a central limitation, and prior acceleration studies have followed three main routes. At the solver level, McNenly et al. [37] reduced the cost of stiff multizone kinetics using approximate Jacobians and Krylov-based preconditioning, reporting about 35-fold speed-up for a 20-zone case and more than 250-fold for 40 zones while preserving accuracy. At the model-structure level, Kodavasal et al. [27]developed AMECS, in which zonal thermal stratification is inferred from a single motored CFD case; with a 40-zone formulation and a 33-species reduced mechanism, reacting simulations were reported to require about one minute. At the chemistry-representation level, Zhou et al. [38] introduced the AGI framework, which replaces online detailed chemistry with interpolation from precomputed databases and was reported to accelerate HCCI calculations by 100 × to more than 10,000 × with CA50 errors generally below 0.7 CAD. Although these figures are not directly comparable because of differences in combustion mode, mechanism size, and model assumptions, they show that substantial runtime reductions are achievable through fundamentally different acceleration strategies.

However, these strategies also involve different trade-offs. Solver-oriented approaches retain detailed online chemistry but have mainly been demonstrated for generic multizone kinetics problemsmcne [37], whereas AMECS and AGI obtain larger speed gains by simplifying thermal stratification or shifting chemistry cost offline [27,38]. Such assumptions are effective for HCCI-type formulations, but they are less straightforward for predictive RCCI applications, where variable fuel blends, strong reactivity stratification, injection-driven state changes, and evolving interzonal heat and mass transport must all be resolved consistently to preserve combustion and exhaust-emission predictivity. This distinction is especially important for large-bore marine RCCI frameworks such as UVATZ, in which improved physical fidelity has been achieved together with increased computational cost [39].

Taken together, the literature shows that chemical-kinetics-based multizone models can predict RCCI combustion behavior and major exhaust-emission trends with useful fidelity, and recent UVATZ developments have further improved their physical realism and integration with full engine-system simulations [2]. However, the central unresolved limitation remains numerical scalability: in detailed RCCI multizone simulations, stiff chemical kinetics must be solved repeatedly in every zone while remaining coupled to interzonal heat and mass transport, causing computational cost to increase rapidly with both zone number and chemical-mechanism size. Existing acceleration studies have demonstrated important progress, but they either target generic multizone kinetics solvers [37]or rely on HCCI-oriented assumptions such as fixed thermal stratification or pre-tabulated/interpolated chemistry [27,38], which do not directly resolve the requirements of predictive multi-fuel RCCI simulation in large-bore marine engines. Therefore, a clear research gap remains in developing a numerically efficient solver strategy that preserves the predictive capability of detailed UVATZ-type multizone models while improving their computational efficiency and scalability. The present study addresses this gap by introducing an accelerated implicit–explicit solution strategy for the UVATZ RCCI framework, designed to decouple the dominant stiffness associated with chemistry and interzonal transport and thereby reduce simulation runtime without compromising predictive accuracy.

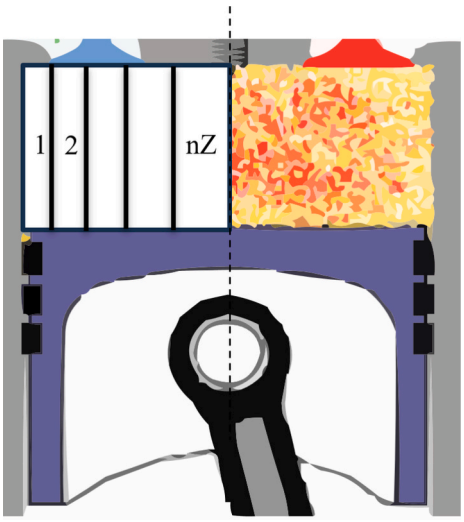

Fig. 1. Typical zone geometries under the annular onion-skin.

Methodology

In the UVATZ framework a coupled system of chemical and physical equations for all zones is solved at each time step. In the present study, the UVATZ model with 13-zone is selected due to its simpler interzonal interactions, which offer greater potential for computational acceleration through the decoupling of chemical and physical solvers. This configuration can still incorporate advanced turbulence features, as these are not dependent on the presence of disc-shaped zones.

The following sections describe the governing equations and key assumptions underlying the new solver in detail.

Governing equations and common assumptions

In the UVATZ framework, the combustion chamber volume is discretized into zones modeled as homogeneous reactors, each with independent thermodynamic states (Fig. 1). These zones are defined by boundaries that separate them from adjacent zones or from the engine surfaces, serving as interfaces for the exchange of heat, mass, and work. A key assumption of MZM is that pressure remains uniform across all zones throughout the simulation. This assumption is justified by the rapid pressure equilibration between zones, which occurs at approximately the speed of sound. As a result, momentum conservation is considered inherently satisfied and is not explicitly included in the governing equations [1] The MZM is governed by a coupled set of equations, which can be classified into chemical and physical transport

equations.

Chemical equations

In the combustion process, chemical kinetics determines the rate of reactions, specifically the rate of generation and consumption of species as well as the thermodynamic state in a zone. Naturally, the fuel oxidation process includes several intermediary species and reactions leading to the final combustion products such as H_2O, CO, CO_2, and NO_X. Thermo-physical and chemical conditions govern these kinetic processes and the elemental reaction rates. Information about the basic reactions, species included, the rate law, and rate constants is stored in the chemical kinetic mechanism. The mechanism file provides data for Eq. (1), determining the total production rate of species i. ν'_{ij} and ν''_{ij} represent forward and reverse stochiometric coefficients. The net reaction rate is calculated via Eq. (2), where k'_j and k''_j are the forward and reverse rate constants, which can be achieved by the Arrhenius relation and equilibrium constant. The heat released because of the changing composition is described in Eq. (3).

$$\dot{\omega}_i = \sum_{j=1}^{n_R} (\nu''_{ij} - \nu'_{ij}) g_j \tag{1}$$

$$g_j = k'_j \prod_{i=1}^{n_S} [X_i]^{\nu'_{ij}} - k''_j \prod_{i=1}^{n_S} [X_i]^{\nu''_{ij}} \tag{2}$$

$$\frac{dE}{dt} = \frac{dm}{dt} e + m\left(c_v \frac{dT}{dt} + \dot{Q} - \dot{W} \right) \tag{3}$$

Physical equations

As derived by Vasudev et al. [1], for each zone, certain equations can be written for mass balance (Eq. (4)), energy balance (or the first law of thermodynamics, Eq. (5)), species balance (Eq. (3)), and the ideal gas Eq. (Eq. (12)). During closed-cycle operation (i.e., when the valves are closed), the injected high-reactivity fuel ($\dot{m}_{\mathrm{inj},z}$) is the only external contribution to the mass balance. The second term represents the interzonal mass transfer. Zones are assumed to contain a constant portion of the cylinder mass.

$$\frac{dm_z}{dt} = \dot{m}_{inj,z} - \sum_i \left(\dot{m}_{i,z-1\to z} - \dot{m}_{i,z\to z+1} \right) \tag{4}$$

In the right side of the energy balance equation, the first term stands for the piston and the interzonal boundaries' work transfer. Wall heat loss (Eq. (6)) is calculated via the modified Woschni correlation by Chang et al [40]. The heat transfer coefficient (hz) is computed according to the thermodynamic state of each zone. Wall temperatures (three values for cylinder head, liner, and piston) are considered given by postprocessing experimental data via the GT-Suit wall temperature solver. Radiation effect is neglected due to low soot characteristic of RCCI [1]. The third term captures the effect of fuel evaporation, and the other terms are regarding interzonal heat transfer which is assumed to be the superposition of two phenomena: temperature gradient and enthalpy transfer due to interzonal species flow [1]. Eq. (7) formulates the conductive heat transfer between adjacent zones in cylindrical configuration.

$$\begin{aligned} \frac{dE}{dt} = & -P_{cyl}\frac{dV_z}{dt} - \dot{Q}_{HL,z} - \dot{m}_{inj,z} q_{evp,z} + \dot{Q}_{z-1\to z} - \dot{Q}_{z\to z+1} \\ & + \hbar_{z-1} \sum_i \dot{m}_{i,z-1\to z} - \hbar_z \sum_i \dot{m}_{i,z\to z+1} \end{aligned} \tag{5}$$

$$\dot{Q}_{HL,z} = h_z A_z (T_z - T_{wall}) \tag{6}$$

$$\dot{Q}_{z\to z+1} = \frac{\pi L (T_{z+1} - T_z)}{\underbrace{\ln\left(\frac{r_{z+1}}{r_z + \frac{\Delta r_z}{2}}\right)}_{\Lambda_{z+1}} + \underbrace{\ln\left(\frac{r_z + \frac{\Delta r_z}{2}}{r_z}\right)}_{\Lambda_z}} \tag{7}$$

The species balance in Eq. (8) consists of terms representing chemical reactions, injected fuel, and interzonal composition diffusion. Diffusion follows Fick's law which can be written in cylindrical space as Eq. (9). Diffusion coefficient can be calculated by Eq. (10) with unity Lewis number assumption.

$$\frac{dY_{i,z}}{dt} = \frac{1}{m_z}\left[-Y_i \frac{dm_z}{dt} + \frac{\dot{\omega}_{i,z} W_{i,z}}{\rho_z} + \dot{m}_{inj,z} Y_{diesel} + \dot{m}_{i,z-1\to z} - \dot{m}_{i,z\to z+1} \right] \tag{8}$$

$$\dot{m}_{i,\,z\to z+1} = \frac{\pi L (\rho_{z+1} Y_{i,z+1} - \rho_z Y_{i,z})}{\underbrace{\ln\left(\frac{r_{z+1}}{r_z + \frac{\Delta r_z}{2}}\right)}_{D_{z+1}} + \underbrace{\ln\left(\frac{r_z + \frac{\Delta r_z}{2}}{r_z}\right)}_{D_z}} \tag{9}$$

$$D_z = \frac{k}{\rho_z c_p} \tag{10}$$

Eqs. (11) and (12) guarantee the uniform pressure (P_{cyl}) condition of the cylinder. Zones can be freely compressed or expended to maintain a uniform pressure while keeping the overall volume equal to the cylinder volume.

$$\sum_{z=1}^{nZ} V_z = V_{cyl} \tag{11}$$

$$P_{cyl} = \frac{1}{V_{cyl}} \sum_{z=1}^{nz} m_z \frac{R_u}{W_z} T_z \tag{12}$$

As shown in Fig. 1, in this study, the zones are defined as concentric cylindrical spheres, starting from the liner [1].

Solution algorithm for acceleration

Multizone Combustion Modeling in Cantera

As explained earlier, the present solver is fully implemented using the UVATZ MZM code, written in C++ and built upon the Cantera framework for solving chemical and thermodynamic equations. Piston motion, direct fuel injection, and wall heat transfer are handled through Cantera's built-in classes and methods, offering reliable and robust functionality. However, for interzonal transport phenomena—such as mass transfer based on Fick's law, heat conduction governed by Fourier's law, and exchange of pressure, volume, work, and enthalpy—dedicated subroutines have been developed and integrated into the original code to extend its capabilities for multizone combustion modeling.

Combustion in a multizone environment is modeled by treating each zone as an interconnected reactor characterized by its own temperature, pressure, and composition. Cantera uses the CVODES solver from the SUNDIALS suite to handle the stiff ODEs governing the time evolution of these reactors [41]. This integration employs adaptive time-stepping and implicit methods, specifically backward differentiation formulas (BDF), to ensure numerical stability and accuracy. The solver relies on Newton's method, where the Jacobian matrix—representing partial derivatives with respect to state variables—plays a central role. Since Jacobian is typically sparse in large systems, specialized sparse matrix solvers are employed to optimize computational performance.

Reaction rate coefficients are fitted using the Chebyshev polynomial method, which ensures efficient and accurate interpolation over a wide range of temperatures and pressures. Cantera performs time integration

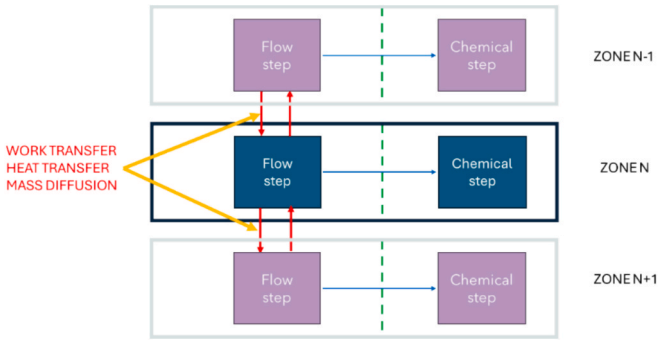

Fig. 2. Schematic Solution Procedure at Each Time Step.

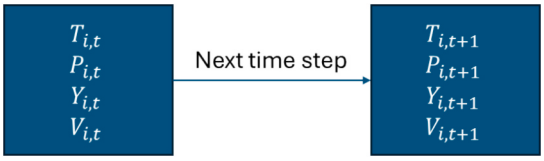

Fig. 3. Schematic of data transfer for each zone (i) at every time step (t) during time marching.

Fig. 4. Schematic for Chemical Step at Each Time Step.

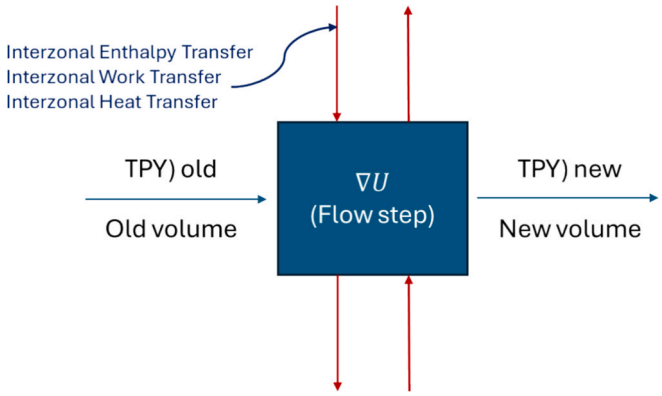

Fig. 5. Schematic for Flow Step at Each Time Step.

using CVODE, supporting both implicit (BDF) and explicit (Adams-Moulton) schemes [42]. For stiff problems, CVODE uses implicit BDF, solving nonlinear systems at each time step via Newton's method. Jacobians are either numerically approximated or internally managed, unless provided analytically by the user. Each reactor (zone) is integrated independently, with the Cantera reactor network managing inter-zone coupling and time advancement. Thus, Cantera delegates all low-level tasks—Jacobian evaluation, Newton iteration, stiffness detection—to CVODE, ensuring robust and efficient chemical kinetics simulation.

At the end of each chemical integration step, cylinder pressure is computed using a Dalton-based ideal-gas multi-zone pressure closure, where contributions from all zones are summed according to their mass, molecular weight, and temperature. This ensures a thermodynamically consistent pressure across zones while preserving the total mass. Currently, the physical solver uses a fixed time step, which is adequate for the present cases. Future improvements may include adaptive time-stepping based on pressure gradients or work transfer rates to enhance accuracy and efficiency. While the multi-zone pressure formulation captures the main pressure dynamics, small discrepancies observed during late-stage ignition in Zone N indicate that energy redistribution via zone work transfer may still be non-negligible. Future work will explore iterative equalization schemes that adjust both volumes and temperatures while conserving zone enthalpy to further reduce these discrepancies.

To accelerate simulation, zone-wise parallelization was implemented using OpenMP on a shared-memory architecture. All chemical integrations are processed concurrently across zones, corresponding to the number of available physical cores. MPI was not used in this study, as all simulations were executed on a single workstation.

Separation of chemical and physical equations

Time integration method in Cantera solver addresses the complex behavior of interconnected reactors by solving governing equations through chemical and physical steps as described in section 2.1. The chemical step involves detailed chemical kinetics to calculate species net production rates, the first law of thermodynamics to determine temperature, and the ideal gas law to calculate pressure, all of which depend on reaction mechanisms, reactant concentrations, temperature, and pressure. The physical step incorporates mass transport by diffusion, enthalpy transfer via species transport, conduction heat transfer, and interzonal work and heat transfer. Fig. 2 illustrates the schematic solution procedure for every time step, where the output of temperature, pressure, species mass fraction, and new zone volume is passed to the next time step as depicted in Fig. 3. This robust framework ensures accurate predictions of thermodynamic states, species concentrations, and transport phenomena within the reactor system, accounting for all significant interactions and dynamics.

Based on the aforementioned rationale and procedural framework for handling and transmitting data, it appears feasible to employ less time-intensive algorithms for addressing the reactor networks by alleviating Jacobian matrix rigidity through implicit methods. Implementing this concept involves segregating physical equations from chemical solutions akin to an HCCI combustion zone within chemical simulations. Meanwhile, the physical equations would govern the solution in subsequent correction steps at each time interval. Executing this promising approach necessitates a thorough grasp of inter-zone transport phenomena to validate the explicit approach and enhance accuracy of solutions.

Therefore, by segregating chemical and physical equations and thoroughly mastering their application, a promising solution can be achieved to reduce computational time while maximizing accuracy. Consequently, the initial step involves solving the chemical equations to disrupt equilibrium conditions and pressure equalization. As previously discussed, time integration utilizing a reduced Jacobian stiffness matrix handles the chemical reactions (depicted in Fig. 4) as the chemical step. This method acquires temperature (T), pressure (P), and mass fractions (Y) along with zone volume (V) from the preceding time step, while the outputs of the physical step serve as initial conditions. It proceeds to solve equations encompassing energy (1st law of thermodynamics), the Arrhenius equation, the ideal gas equation of state, and chemical reactions, thereby updating T, P, Y, and V changes influenced by piston motion, which applies total work across all zones.

Now, the results derived from solving the chemical step are utilized as input values for the physical step. Instead of resolving all equations implicitly, a thorough understanding and precise solution of transport phenomena between each zone are crucial. Consequently, each zone is treated as an open thermodynamic system to update its internal energy (U), forming the basis for addressing physics during the correction step.

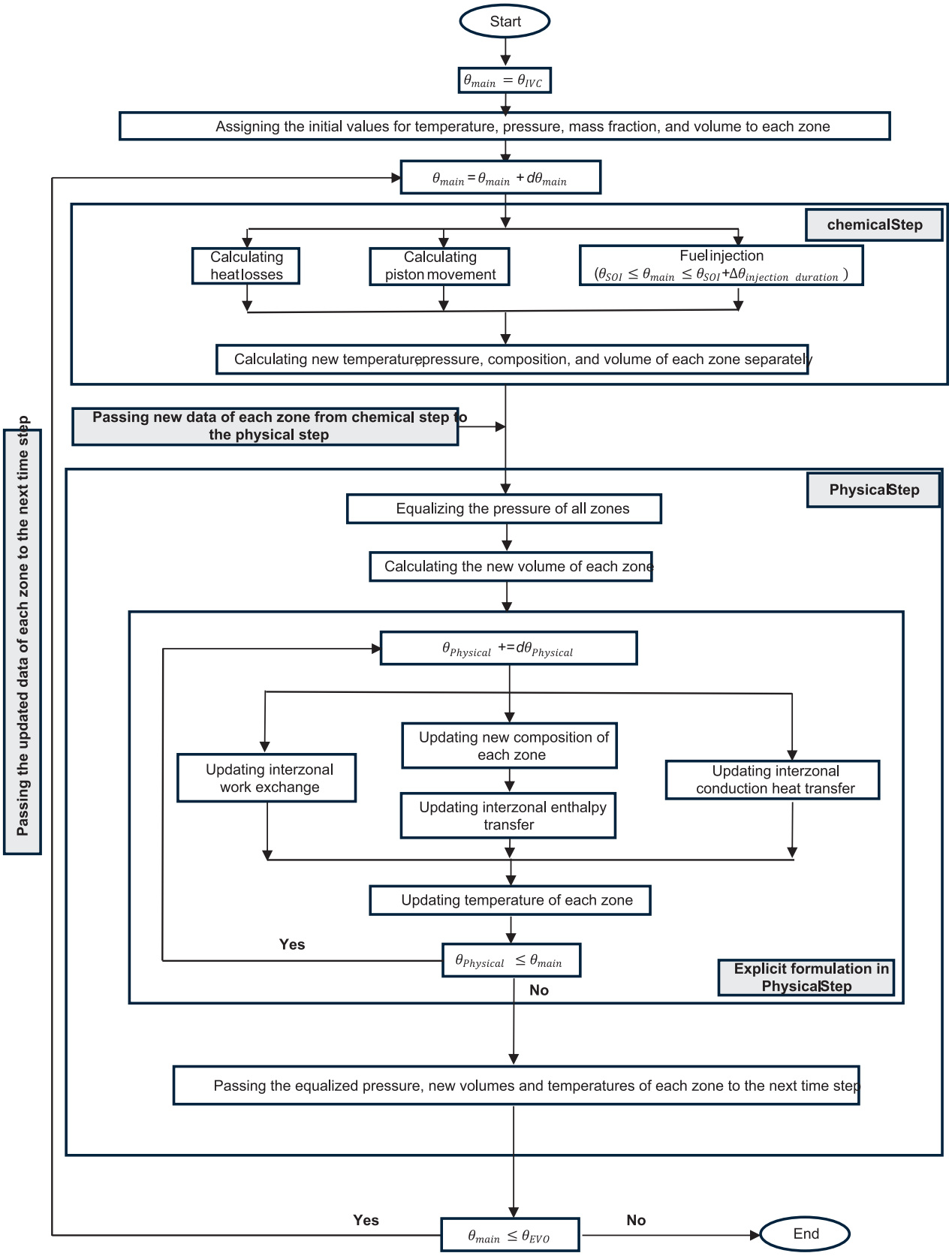

Fig. 6. Algorithm of solution procedure.

Table 2
Operating points from the SCRE for model comparison, including the error of UVATZ in predicting their key performance indexes.

Case	Load [%]	BR [pp]	SOI [CAD]	λ [-]	Tint [K]	Pint [bar]	Pmax error [%]	IMEP error [%]	NHR error [%]
1 (A from [35])	11	Ref −42	Ref −65	+1.8	Ref	Ref + 0.5	2.7%	1.5%	1.5%
1 (B from [35])	25	Ref −11	Ref −65	+1	Ref	Ref + 1.3	1.3%	0.5%	4.8%
1 (D from [35])	50	Ref + 2.4	Ref −65	+0.8	Ref-5	Ref + 3.5	3.7%	0.1%	2.7%

This approach entails accounting for all thermodynamic conditions such as enthalpy transfer, conductive heat transfer, and interzonal work among neighboring zones. Enthalpy transfer between zones for each species necessitates solving the mass transport through diffusion beforehand. This entire process is illustrated in Fig. 5, highlighting the iterative nature and interdependence of chemical and physical processes within the reactor system. In this procedure, T, P, Y, and V obtained from the chemical step are updated through energy equation of a close thermodynamic cycle, pressure equalization method, diffusion mass transfer equation, and the ideal gas equation of state in the flow step. The updated values then progress to the subsequent time step.

The variation of species mass fractions within each computational zone is governed by both chemical reactions and diffusion processes. The system of ordinary differential equations (ODEs) describing the chemical kinetics is discretized using a first-order Euler method. The integration involves solving the Arrhenius equation to compute the reaction rates, which are then used to update the mass fractions of each species.

A key aspect of this chemical integration step is that, although the solution procedure is implicit, the reaction rate equations for all zones are fully decoupled. This decoupling significantly reduces the size of the coefficient matrix, leading to lower memory requirements and computational cost compared to fully coupled approaches.

In contrast, during the physical transport step, an explicit scheme is employed for the diffusion term. This choice is made to preserve numerical accuracy, as diffusion processes are highly sensitive to the time step size, and implicit schemes may introduce excessive numerical diffusion or damping.

Phenomena of interzonal interaction

As previously explained, the interzonal interactions that make the Jacobian matrix highly stiff are decoupled to reduce simulation runtime. The physical step is responsible for this decoupling process, solving the interzonal interactions explicitly. The physical phenomena addressed through time integration method to simulate the reactor networks include interzonal mass transfer, enthalpy transfer, heat transfer, direct fuel injection, evaporation of direct injection fuel, and work. By decoupling the chemical and physical steps, the time integration method is not only responsible for solving chemical reactions but also for performing certain generic physical steps. These include heat loss from the boundaries (such as the cylinder head, liner, and piston), piston movement (applying total work to the mixture) and managing fuel injection during the injection duration.

A key insight from the decoupling procedure is the introduction of an additional time step for the physical process. There is no adaptive time-stepping strategy in the physical step. However, such a strategy exists in the chemical step, where the specified time step serves as the initial value. In contrast, the physical step treats it as a fixed value. Although implementing adaptive time stepping in the physical step is possible, using criteria such as the maximum Courant number, as commonly done in computational fluid dynamics (CFD), it would require careful consideration, especially since there are no convection effects in the zones that would typically respond sensitively to changes. However, decoupling this approach eliminates its adaptive capability, necessitating an auxiliary time step to preserve accuracy and mitigate the risk of numerical divergence. The physical time step can be set equal to or shorter than the primary time step used for the chemical process and time integration scheme. A shorter physical time step in the explicit treatment of governing equations ensures numerical accuracy and stability. This time step governs all transient transport phenomena, including mass diffusion, enthalpy transfer, and conductive heat transfer. While reducing the physical time step relative to the main time step used in the chemical process improves accuracy, it also increases computational cost.

A key enhancement of the new code is its ability to fully decouple the computations for all zones, enabling parallel execution of both the chemical and physical steps independently. This is achieved by breaking down the implicit matrix into smaller, zone-specific matrices, with the number of matrices equal to the number of computational zones. As a result, each zone can be solved independently, which significantly improves scalability and parallel efficiency.

It is important to note that for large chemical mechanisms, the computational cost of the chemical step increases exponentially with the number of species and reactions. Therefore, this decoupled approach not only reduces memory usage but also makes the solver more practical and efficient for complex reaction mechanisms. Since only specific processes, such as those involving access to non-common variables like zone-specific variables, are executed in parallel, high shared-memory efficiency is expected.

The physical time step, which is shorter than the main time step used in the chemical step, accumulates precisely to match the overall time advancement of the simulation. It governs all physical transport equations, including interzonal interactions, and provides updated values for T, P, Y, and V. These updated quantities serve as input for both the subsequent time step and the next chemical step.

It is important to distinguish between the pressure output from the chemical step—which varies across zones—and the pressure after the physical step, which is uniform across all zones. This distinction underscores the role of the physical step as a *correction step*.

In the present study, the code is developed for the annular onion-skin multi-zone model, as illustrated in Fig. 1. However, the methodology can be generalized to other types of zone geometries. The solution procedure follows a sequential approach during each physical step iteration: first, pressure is equalized, followed by volume updating, wall movement, interzonal transport phenomena, and finally, temperature updating. At this stage, the updated values of pressure, temperature, species composition in each zone, and zone volumes are determined. As previously discussed, these quantities are then propagated to the subsequent time step. A schematic representation of the problem-solving algorithm is provided in Fig. 6.

Scope of research

To evaluate the accelerated solver against the existing one, three operating points from real SCRE measurements are selected, two from Kakoee et al. [35]and one additional 50% load case. Table 2 presents data relative to a reference value (ref), corresponding to a standard IMO (international maritime organization) Tier III low-load calibration point for the commercial Wärtsilä W31DF, a multicylinder dual-fuel, lean-burn NG-diesel engine. Kakoee et al. [35] demonstrated that UVATZ predicts peak pressure within 5% and CA50 within 1.4 CAD of experimental results for these cases. The relative error of key performance indexes in comparison to the experimental data is also mentioned in Table 2. Readers are referred to the original work for more details. These same points have been used in other model developments (e.g.,

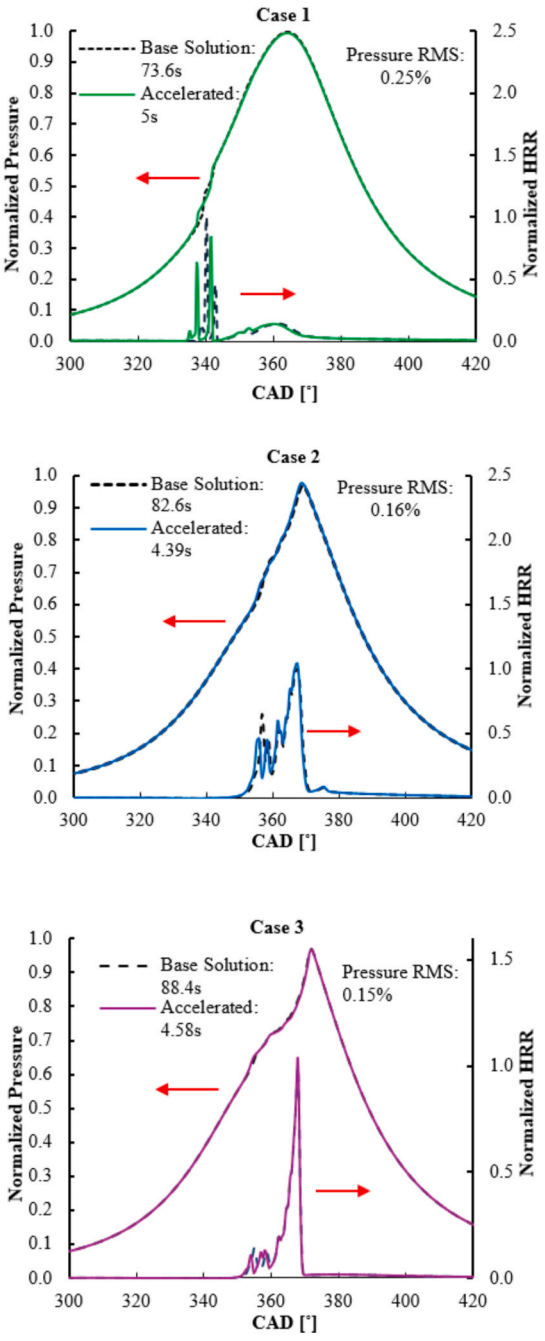

Fig. 7. Normalized pressure curves comparison between the accelerated solver and the base solver.

aftertreatment and control [43]), reinforcing the base model's reliability and robustness.

The chemical kinetics are handled using the mechanism of Yao et al. [41] which includes 54 species and 269 reactions. This mechanism is referred to as the SK54 mechanism in this work. The high-reactivity fuel (diesel) is represented by n-dodecane ($nC_{12}H_{26}$), while methane (CH_4) is used as the low-reactivity fuel. This section compares the results of the new accelerated method with those of the baseline solution, which uses the original UVATZ structure [34]. In the present study, accuracy refers to how closely the new method's results match the baseline, while speed-up is defined as the ratio of run-times between the baseline and the accelerated solver.

Table 3
Runtime, accuracy and speed-up for 3 different engine loads with base and new methods.

Case No.	Base runtime (s)	Accelerated runtime (s)	Speed up (times)	P. RMS (%)
1	73.6	5	14.7	0.25
2	82.6	4.39	18.8	0.16
3	88.4	4.58	19.3	0.15

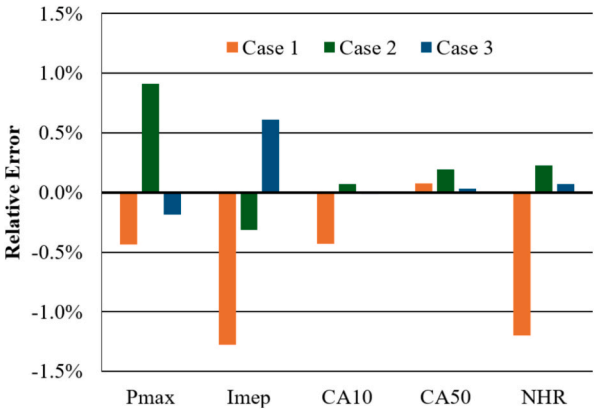

Fig. 8. Relative difference of engine indicators calculated by accelerated solver.

Results and discussion

In this part, an explicit solver is used to solve the transport equation between zones. The timestep for the chemical solver and data writing is considered equal to 0.2 crank angle. However, for the heat and mass transfer, at least 10 smaller steps are considered after each chemistry step. This is essential to maintain convergence and provide a proper agreement with the implicit solution. The Intel(R) Core (TM) i7-13700H 2.40 GHz processor (with a maximum 20 parallel threads) is utilized to execute simulations.

In the explicit physical step, each computational zone is treated as an open system, where mass and energy exchange with neighboring zones is computed using finite-difference discretization. The solver updates the thermodynamic state variables, temperature, pressure, species mass fractions, and volume (T, P, Y, V), by solving transport equations that account for diffusion, heat conduction, and interzonal work. Once this step is completed, the updated state variables are passed to the chemical step. This decoupled approach, explicit for transport and implicit for chemical kinetics, improves computational efficiency, particularly when simulating complex combustion mechanisms involving numerous species.

Acceleration of the base cases

Fig. 7 compares the pressure and heat release rate (HRR) results from solvers using the base and accelerated codes. It can clearly be seen that the accelerated solver closely follows the base results across three different cases.

Fig. 7 also shows the runtime for both base and accelerated codes. For a better comparison, the acceleration results are also summarized in Table 3. It is seen that up to about 20 × speed-up has been achieved for the mentioned cases.

To further evaluate the accuracy of the results of the new method, key engine parameters—including maximum cycle pressure (Pmax), IMEP, CA10, CA50, and net heat release (NHR)—obtained from both solvers are compared in Fig. 8. As shown, engine performance indicators remain within a 1.5% error margin, demonstrating the reliability of the

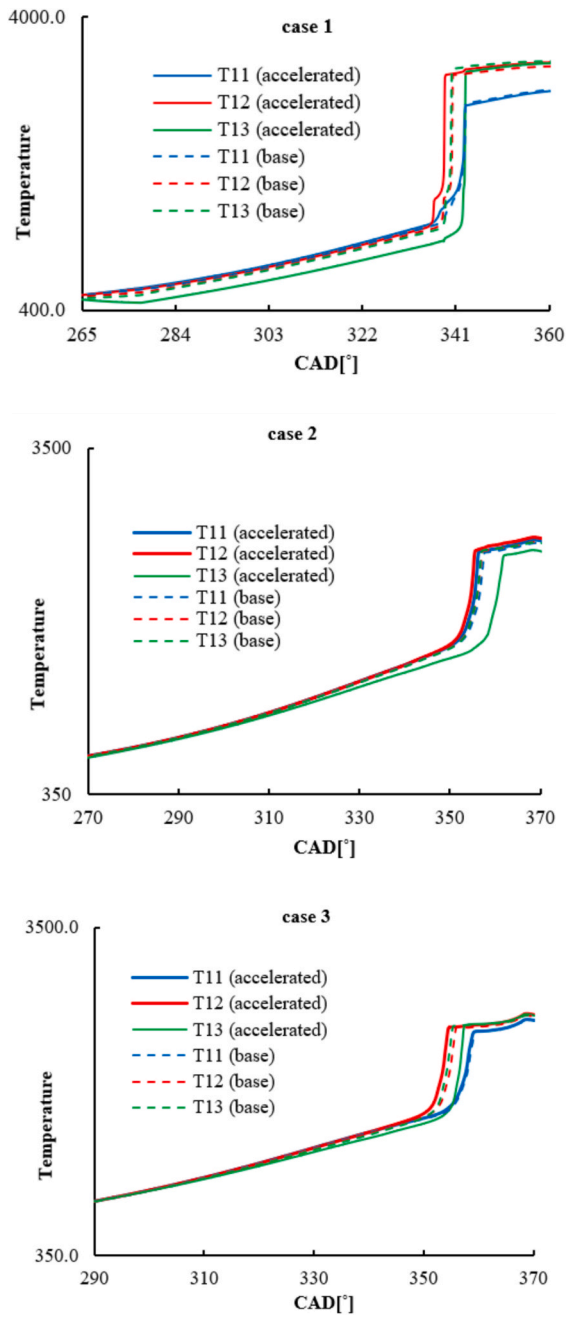

Fig. 9. Temperature of the three last zones near the cylinder wall over crank angles close to the start of combustion.

new method for engine operation prediction.

From Fig. 7, minor deviations can be observed at points with a high-pressure rise, which is typically expected from an explicit solver. Considering the heat release rate results, it is evident that these deviations become especially pronounced when combustion initiates abruptly, causing significantly high temperature gradients between zones. To gain more insight into the zonal comparison between the base and accelerated methods, Fig. 9 presents the temperatures of the last zones for all cases. Although a logarithmic scale is used to display temperatures, the sharp temperature rise at the start of combustion remains evident. While the temperature trends are similar after the end of zonal combustion, the last two zones (closest to the cylinder wall) behave differently in the two simulations. In the base method, the last two zones ignite simultaneously, whereas in the accelerated method, combustion initiates first in the 12th zone before the 13th. This behavior

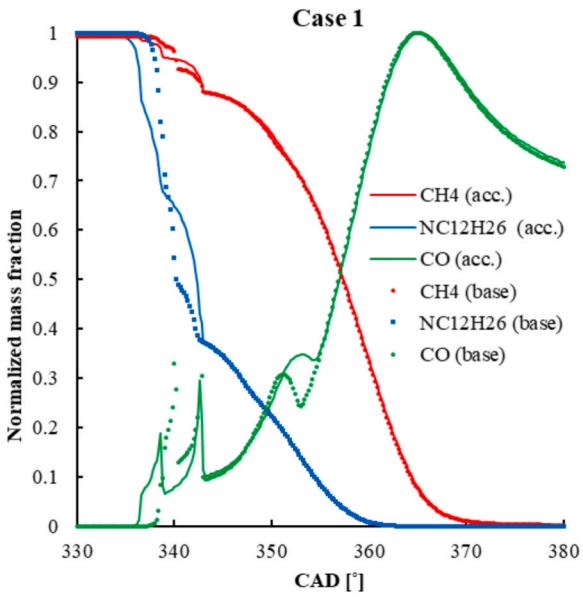

Fig. 10. Comparison of unburned methane and diesel levels, between the two methods over crank angles near the start of combustion.

mainly stems from temperature differences established during the injection phase. Due to varying amounts of fuel vapor added to the zones, their pressures rise unevenly. As explained in the methodology section, pressure equalization in the accelerated solver is performed using a Dalton-based ideal-gas multi-zone pressure closure, where each zone contributes according to its mass, molecular weight, and temperature. Because this formulation does not assume uniform temperature, uneven temperature distributions persist when heat transfer between zones is slower than work transfer, particularly during late-stage ignition. Nevertheless, Fig. 9 shows that the effect of this irregularity diminishes as combustion propagates to other zones. Moreover, this phenomenon appears to be confined to the last zones where a high fuel distribution gradient exists, as demonstrated by the 11th zone temperatures, where the results of the two simulations closely match.

Crank-angle-resolved mass fractions further support the above explanations. Fig. 10 shows the behavior of fuel species (CH4 and nC12H26) during the simulations for case 1, which exhibits the most deviations. It is evident that diesel combustion starts later in the accelerated code due to the earlier combustion of the 12th zone. However, as the simulation progresses, the results align with the base solution,

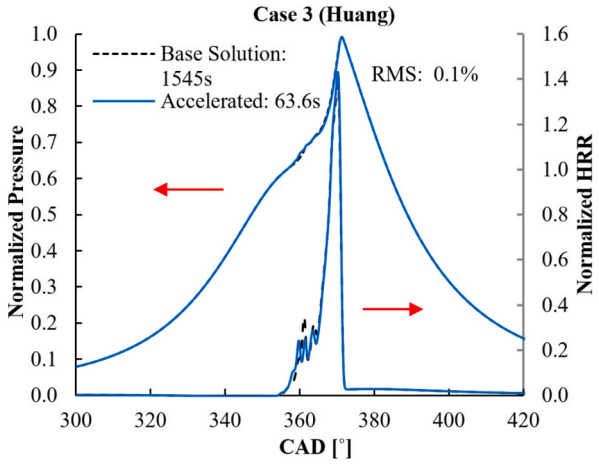

Fig. 11. Normalized pressure curves comparison between the accelerated solver and the base solver with Huang et al. [44] mechanism.

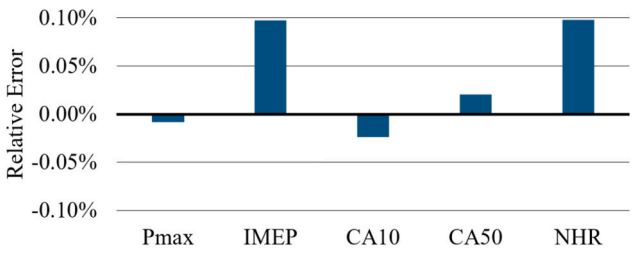

Fig. 12. Relative difference of engine indicators calculated by accelerated solver for Huang et al. [44] mechanism.

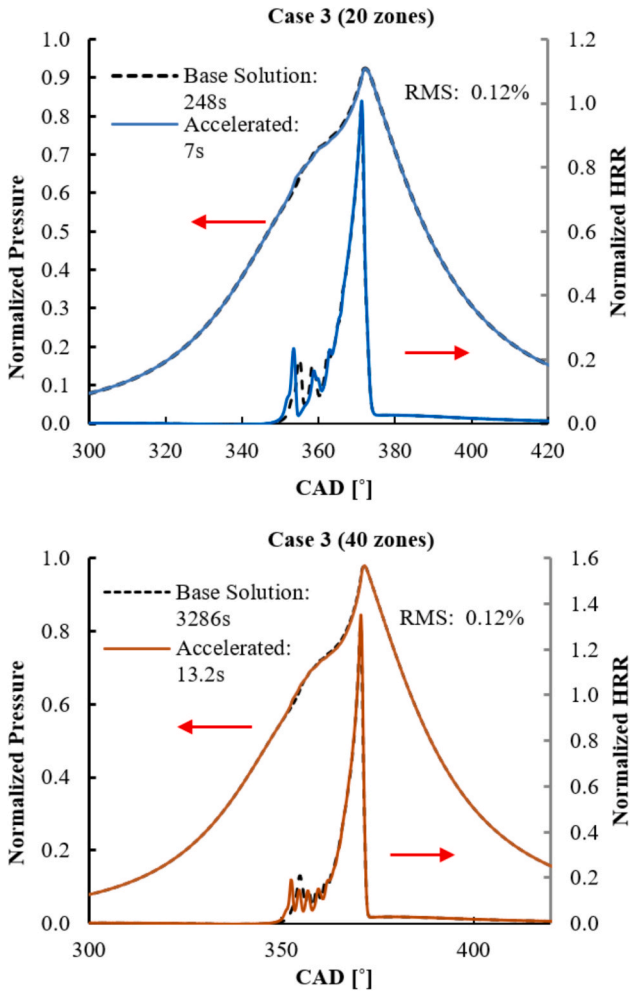

Fig. 13. Normalized pressure curves comparison between the accelerated solver and the base solver in different number of zones.

leading to good agreement in other performance measures. The CO results show the same trend in addition to another deviation between 350 and 360 crank angles. This is also justifiable by the decoupled nature of chemical equations and transport equations. Again, the model's capability of emission prediction is untouched as the curves ultimately converge to a similar shape.

The results show that the method performs well in predicting species formation and consumption, demonstrating its reliability for the prediction of all emission species included in the employed chemical kinetics mechanism.

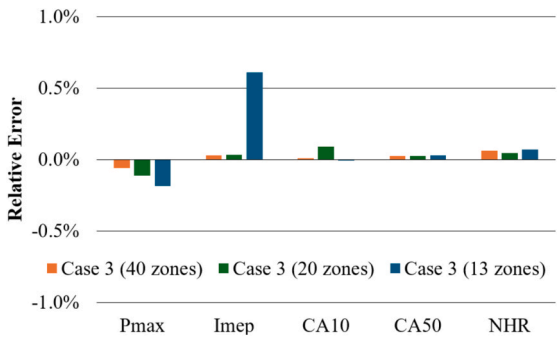

Fig. 14. Relative difference of engine indicators calculated by accelerated solver in different number of zones.

Handling mechanism complexity

To demonstrate the method's effectiveness in handling more detailed mechanisms (that improve simulation accuracy), the solvers were also tested with a larger mechanism. For this comparison, case 3 from Table 2 was selected and simulated with both methods. As shown in Figs. 11 and 12, better conformity between the results and a higher acceleration (approximately 24 ×) were achieved when the kinetic mechanism was replaced with a larger one developed by Huang et al [44]. This mechanism corresponds to the reduced GXU dual-fuel kinetic mechanism, which contains 143 chemical species and 746 elementary reactions. The mechanism was constructed by integrating several reduced sub-mechanisms. First, a base n-heptane mechanism derived from the reduced primary reference fuel (PRF) mechanism of Wang et al. (73 species and 296 reactions) was used as the core diesel oxidation framework after removing *iso*-octane and toluene related reactions. Second, a reduced n-butylbenzene mechanism, originally derived from a detailed mechanism containing 960 species and 4330 reactions, was generated using directed relation graph with error propagation (DRGEP), rate-of-production (ROP) analysis, and sensitivity analysis. Third, a reduced natural gas sub-mechanism based on the detailed mechanism of Healy et al. (293 species and 1588 reactions) was similarly reduced using DRGEP, ROP, and sensitivity analysis. In addition, a reduced PAH (polycyclic aromatic hydrocarbon) sub-mechanism was incorporated to represent soot precursor formation, and a simplified NOx sub-mechanism consisting of 4 species and 12 reactions was included to describe NOx formation through thermal and N_2O-intermediate pathways. Diesel fuel in the mechanism is represented by a surrogate mixture of n-heptane and n-butylbenzene, while natural gas is represented by a mixture of methane, ethane, and propane. After merging the individual sub-mechanisms and removing duplicate reactions, the final reduced GXU mechanism contains 143 species and 746 reactions, and it has been validated against ignition delay times, laminar flame speeds, and HCCI engine combustion data, demonstrating good predictive capability for dual-fuel combustion simulations.

Sensitivity to zonal resolution

The new method provides greater speed-up with an increasing number of zones. As the number of zones grows, the acceleration improves, as shown in Fig. 13. In a 40-zone configuration, the accelerated

Table 4
Runtime and speed-up for different number of zones with base and new methods.

Number of zones	Base runtime (s)	Accelerated runtime (s)	Speed up (times)
13	88.4	4.58	19.3
20	248	7	35
40	3286	13.2	249

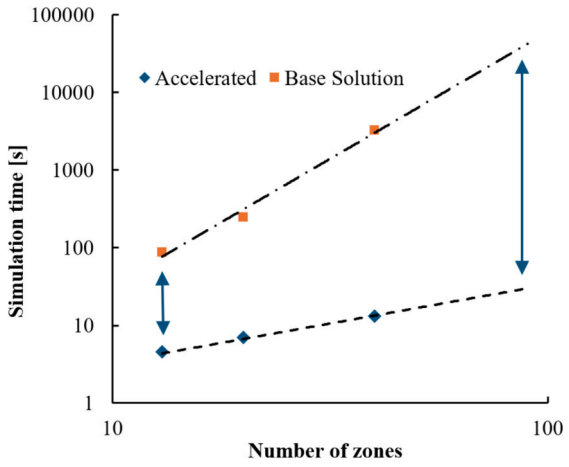

Fig. 15. Graphs comparing the runtime across different numbers of zones for solver with base method and new method.

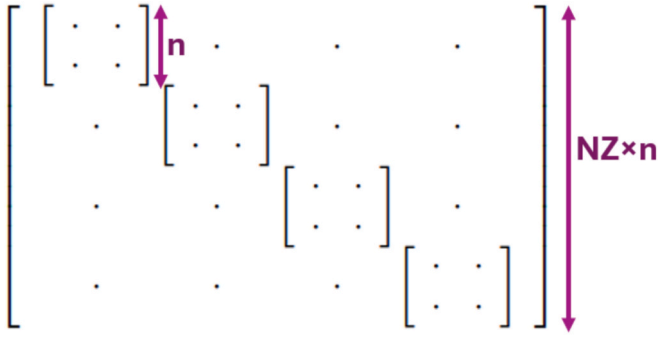

Fig. 16. Comparison of the equation matrix sizes for a single zone versus the entire system.

solver is 249 times faster. Furthermore, as shown in Fig. 14, higher zonal resolution results in smaller differences in the predicted engine indicator parameters. To further demonstrate the method's performance in achieving speed-up with many zones, Table 4 presents the solution times and corresponding speed-ups for case 3 (high load) with 13, 20, and 40 zones.

For a more observative comparison, the runtimes have been presented in graphs in

Fig. 15 Because of extremely different scales and to show the nature of behaviors, the results for the two methods are depicted in logarithmic scale. It can be observed that for the base method, runtime grows as a power function with the number of zones, making it impractical to use a large number of zones. In contrast, with the new method, runtime increases linearly, making it feasible to employ a larger number of zones to achieve higher accuracy.

Sources of code acceleration

Separation of zones: solving smaller matrices

From matrix calculus, it is known that the number of calculations required to invert a matrix of size n is of the order n^3 [45] As shown in Fig. 16, if the number of equations for a single zone is n, the total number of equations for the entire system would be $NZ \times n$, where NZ is the number of zones. Therefore, if n^3 computations are required for a single zone, the number of calculations needed for NZ individual zones would be $NZ \times n^3$. However, for a system of NZ interconnected zones, the number of calculations would be $(NZ \times n)^3$, which is NZ^2 times greater than for the case with separated zones. This estimation demonstrates how separating zones can drastically reduce the number of calculations and speed up simulations.

This also explains the greater speed-up observed with larger mechanisms and a higher number of zones. As the mechanism becomes larger, with more number of species, n increases, and as the number of zones becomes more, the NZ rises. Both factors lead to a larger solution matrix, allowing the new method to demonstrate even better performance.

Table 5
Simulation Time (normalized) for different conditions, with and without Parallelization.

Case no.	Time of Chemical part (normalized)	Total time (normalized)
1	1.60	2.08
2	0.46	1.00
3	20.25	22.15
4	11.71	14.44
5	5.88	7.13
6	1.33	3.00

Enabling the use of optimized solvers for each equation category

In the base solver, the same stiff ODE solver is applied to all equations, both chemical and physical, despite their differing characteristics. In the new method, various strategies can be employed to accelerate the solution of the transport equation between zones. For instance, using optimal solvers tailored to each equation type: a stiff ODE solver for the chemical equations and an explicit (or implicit) finite difference solver for the physical transport equations.

Enabling parallel processing

When using chemical kinetics to solve reactions, a significant portion of time is dedicated to solving these equations within each zone. As the mechanism becomes larger (with more species and reactions), the computational cost increases accordingly. By implementing the proposed approach, separate computational threads can be assigned to different zones, allowing chemical reactions to be solved independently and simultaneously. This approach significantly reduces overall computation time.

To quantify this improvement, the mid-load engine case (described in Table 2) was simulated using the new accelerated method. Two mechanisms were used for comparison: a smaller mechanism (SK54) and a larger mechanism (Huang). Each condition was simulated twice, once without parallelizing the chemical solution across zones, and once with parallelization. The case without parallelizing, has been performed on one CPU core, and for the parallelization, OpenMP library has been used on the CPU with maximum 20 computational threads.

All other simulation parameters, such as time steps, remain consistent across all four simulations. The results are summarized in Table 5. To facilitate a clearer comparison, the simulation times are normalized by dividing them by the time required for Case 2, which is 4.39 s as shown in Fig. 7. The compared cases are as follows:

1. Case 1: Small mechanism (SK54), no parallelization
2. Case 2: Small mechanism (SK54), with parallelization of chemical simulations across zones
3. Case 3: Large mechanism (Huang), no parallelization
4. Case 4: Large mechanism (Huang), with parallelization of chemical simulations across zones
5. Case 5: 40 zones, no parallelization
6. Case 6: 40 zones, with parallelization

The table shows that without parallelization, a significant amount of simulation time is spent on chemical equations, particularly for the larger mechanism. As expected, the case with the larger mechanism needs a higher computation time due to the greater number of species and requires more time for solving physical species transport equations and speed-up due to parallelization for this case is 1.53 times. It can be observed that parallelization results in a substantial speed-up across all

Table 6
Comparison of previous acceleration methods and the present UVATZ-IMEX approach for multi-zone combustion modeling.

Method	Scope	Acceleration route	Online chemistry	Reported gain	Main RCCI limitation
McNenly et al. [37]	Generic MZM kinetics	Approximate Jacobian + Krylov/ preconditioning	Yes	~35× (20 zones), >250× (40 zones)	Not developed for predictive multi-fuel RCCI
AMECS [27]	HCCI MZM	CFD-informed thermal-stratification simplification	Yes	~1 min for 40-zone reacting case	Relies on pre-derived stratification
AGI [38]	HCCI MZM	Interpolation from precomputed chemistry database	No (tabulated/ interpolated)	~100 × to > 10,000×	Limited by database coverage and assumptions
Present UVATZ-IMEX	Large-bore marine RCCI MZM	IMEX decoupling of chemistry and transport; parallelizable zonal solution	Yes	14.7–19.3× (13 zones), ~24× (143 species), 35× (20 zones), 249× (40 zones)	Small local splitting errors possible under strong gradients

cases, with the effect being more pronounced for the smaller mechanism, with 2.08 times speed-up and specially for the model with more zones, with 2.37 times speed-up.

It is worth noting that in methods utilizing tabulated chemical kinetics, such as [25], the chemical computation, which is seen from the table that constitutes a significant portion of the total simulation cost, is designed to be extremely fast and computationally efficient. This results in a much faster overall solution. Thanks to the modular structure of the present method, the chemical solver can be easily replaced with a tabulated kinetics module to further increase computational speed. However, in the current work, the objective has been to develop an MZM-based solver that fully resolves detailed chemical reactions. This allows for accurate modeling of combustion initiation, combustion development, and the formation of all emission species, which are difficult to capture with tabulated approaches. In addition, this method does not require a tabulation code and only needs to be supplied with the reaction mechanism.

Table 6 shows that previous acceleration studies have followed three main routes: solver-level improvement, simplification of thermal stratification, and tabulation/interpolation of chemistry. The present UVATZ-IMEX method belongs to the first category but extends it to predictive large-bore RCCI simulation, where detailed chemistry, interzonal transport, and strong reactivity stratification must be retained simultaneously. While AGI [38] and AMECS [22] report larger gains under HCCI-oriented assumptions, their formulations are less directly applicable to predictive multi-fuel RCCI. The main contribution of the present method is therefore to achieve substantial speed-up while preserving the physical and chemical fidelity required for RCCI analysis.

Conclusions

An accelerated numerical framework was developed for the UVATZ multi-zone RCCI combustion model using an implicit–explicit solution strategy that decouples chemical kinetics from interzonal transport processes. The principal findings are summarized as follows:

- Significant computational acceleration: The proposed solver achieves ≈20 × speed-up using the SK54 mechanism (54 species, 269 reactions) and up to ≈24 × acceleration with a larger 143-species/ 746-reaction mechanism for a 13-zone model, substantially improving computational efficiency.
- Improved scalability with zone number: The baseline implicit solver exhibits cubic runtime growth with increasing zone count, whereas the proposed approach demonstrates near-linear scaling, enabling efficient simulations with larger multizone configurations.
- High predictive accuracy: Despite the substantial speed-up, key combustion indicators (Pmax, IMEP, CA10, CA50, and heat-release characteristics) show deviations below 1.5% relative to the baseline solver. In addition, pressure traces and emissions trends closely match the reference results across the investigated operating conditions.
- Enhanced simulation capability: The accelerated framework enables the practical use of larger chemical kinetic mechanisms and higher zonal resolution, significantly improving the capability of detailed RCCI multizone combustion simulations.
- Model limitation: Minor deviations in heat-release rate and zonal temperature gradients appear under strong fuel-distribution gradients. These differences originate from the explicit decoupling of transport equations and pressure closure from the implicit reactor network through the implicit–explicit operator-splitting strategy used in the accelerated solver.
- Broader applicability: Although demonstrated for RCCI combustion, the proposed solver framework can be extended to other low-temperature combustion strategies such as HCCI and PCCI, where detailed chemical kinetics and multizone modeling are required.

Overall, the proposed framework dramatically improves the computational efficiency and scalability of detailed RCCI multizone simulations while preserving high predictive accuracy, enabling faster and more practical simulation of advanced low-emission engine combustion systems. This framework provides a robust, scalable tool for engineers, accelerating RCCI simulation while preserving accuracy, and paving the way for sustainable engine advancements.

Further investigations are needed to focus on model stability and accuracy under various conditions. Particularly, a reasonable and robust methodology is needed to determine the maximum step size required to ensure stability and accuracy.

CRediT authorship contribution statement

Mohammad Mahdi Salahi: Writing – review & editing, Writing – original draft, Supervision, Software, Methodology, Investigation, Formal analysis, Data curation, Conceptualization. **Jamshid Moradi:** Writing – original draft, Software, Methodology, Conceptualization. **Kian Golbaghi:** Writing – original draft, Validation, Software, Data curation. **Shadab Heidarabadi:** Writing – original draft. **Amin Andwari:** Writing – review & editing, Supervision, Resources, Project administration, Funding acquisition. **JariHyvönen:** Supervision, Resources, Funding acquisition. **Maciej Mikulski:** Writing – review & editing, Supervision, Resources, Funding acquisition.

Declaration of competing interest

The authors declare that they have no known competing financial interests or personal relationships that could have appeared to influence the work reported in this paper.

Acknowledgments

This research was conducted within the framework of the Computationally Aided Systems Engineering for Marine Advanced Technology for The Environment (CASEMATE) project, co-funded by Business Finland (ref. 2911/31/2022) under the Wärtsilä ZEM (Zero Emission Marine) ecosystem. Shadab Heidarabadi also gratefully acknowledges financial support from Fortumin ja Nesten Säätiö (grant no. 20250019).

Data availability

The data that has been used is confidential.

References

[1] Vasudev A, Mikulski M, Balakrishnan PR, Storm X, Hunicz J. Thermo-kinetic multi-zone modelling of low temperature combustion engines. Prog Energy Combust Sci 2022;91. https://doi.org/10.1016/j.pecs.2022.100998.

[2] Vasudev A, Kakoee A, Axelsson M, Almani HM, Hyvönen J, Mikulski M. Advancing autonomy of chemical kinetics based multizone models for reactivity controlled compression ignition engines. Energy Convers Manage 2024;312:118562. https://doi.org/10.1016/j.enconman.2024.118562.

[3] Čampara L, Hasanspahić N, Vujičić S. Overview of MARPOL ANNEX VI regulations for prevention of air pollution from marine diesel engines. SHS Web of Conferences 2018;58:01004. https://doi.org/10.1051/shsconf/20185801004.

[4] S. Heidarabadi, R. Khoshbakhti Saray, and E. Neshat, "Detailed kinetic study on methane/diesel RCCI combustion," *International Journal of Engine Research*, vol. 22, no. 8, pp. 2422–2441, Aug. 2021, doi: 10.1177/1468087420954012.

[5] A. Mohammed Elbanna, C. Xiaobei, Y. Can, M. Elkelawy, H. Alm-Eldin Bastawissi, and H. Panchal, "Fuel reactivity controlled compression ignition engine and potential strategies to extend the engine operating range: A comprehensive review," *Energy Conversion and Management: X*, vol. 13, p. 100133, 2022, doi: https://doi.org/10.1016/j.ecmx.2021.100133.

[6] S. Lahane, P. W. Deshmukh, and M. R. Nandgaonkar, "Mathematical Modeling of Injection and Spray Characteristics of a Diesel Engine: A Review," in *Energy, Environment, and Sustainability*, Springer Nature, 2022, pp. 29–55. doi: 10.1007/978-981-16-8618-4_3.

[7] X. Tauzia, J.-F. Hétet, P. Chessé, B. Inozu, and P. Roy, "The use of a Phenomenological, multizone combusion Model to investigate emissions from Marine diesel engines." [Online]. Available: https://hal.science/hal-01155851.

[8] Dempsey AB, Curran S, Reitz RD. Characterization of reactivity controlled compression ignition (RCCI) using premixed gasoline and direct-injected gasoline with a cetane improver on a multi-cylinder engine. SAE Int J Engines 2015;8(2):859–77.

[9] Benajes J, García A, Monsalve-Serrano J, Balloul I, Pradel G. Evaluating the reactivity controlled compression ignition operating range limits in a high-compression ratio medium-duty diesel engine fueled with biodiesel and ethanol. Int J Engine Res 2017;18(1–2):66–80. https://doi.org/10.1177/1468087416678500.

[10] Ganesan N, Le TH, Ekambaram P, Balasubramanian D, Le VV, Hoang AT. Experimental assessment on performance and combustion behaviors of reactivity-controlled compression ignition engine operated by n-pentanol and cottonseed biodiesel. J Clean Prod 2022;330:129781. https://doi.org/10.1016/j.jclepro.2021.129781.

[11] E. Doosje, F. F. Willems, and R. R. Baert, "Experimental demonstration of RCCI in heavy-duty engines using diesel and natural gas," 2014. [Online]. Available: https://api.semanticscholar.org/CorpusID:109031720.

[12] M. Dahodwala, S. Joshi, E. W. Koehler, and M. Franke, "Investigation of diesel and CNG combustion in a dual fuel regime and as an enabler to achieve RCCI combustion," in *SAE 2014 World Congress & Exhibition*, SAE Technical Paper, 2014.

[13] Mikulski M, Ramesh S, Bekdemir C. Reactivity controlled compression ignition for clean and efficient ship propulsion. Energy 2019;182:1173–92. https://doi.org/10.1016/j.energy.2019.06.091.

[14] M. Elkelawy, E. A. El Shenawy, S. A. Mohamed, M. M. Elarabi, and H. Alm-Eldin Bastawissi, "Impacts of EGR on RCCI engines management: A comprehensive review," *Energy Conversion and Management: X*, vol. 14, p. 100216, 2022, doi: https://doi.org/10.1016/j.ecmx.2022.100216.

[15] Elkelawy M, El Shenawy EA, Mohamed SA, Elarabi MM, Bastawissi H-A-E. Impacts of using EGR and different DI-fuels on RCCI engine emissions, performance, and combustion characteristics. Energy Convers Manage: X 2022;15:100236. https://doi.org/10.1016/j.ecmx.2022.100236.

[16] Paykani A, Kakaee A-H, Rahnama P, Reitz RD. Progress and recent trends in reactivity-controlled compression ignition engines. Int J Engine Res 2016;17(5):481–524. https://doi.org/10.1177/1468087415593013.

[17] A. Soleimani, J. Kim, M. Axelsson, J. Hyvonen, and M. Mikulski, "Exhaust Thermal Management in a Dual-Fuel Marine Engine via Fully Variable Valve Actuation and Wastegate Lambda Control," in *17th International Conference on Engines and Vehicles*, SAE International, Sep. 2025. doi: https://doi.org/10.4271/2025-24-0085.

[18] Fakhari AH, Gharehghani A, Salahi MM, Andwari AM. Numerical investigation of the hydrogen-enriched ammonia-diesel RCCI combustion engine. Fuel 2024;375:132579. https://doi.org/10.1016/j.fuel.2024.132579.

[19] Kim J, Soleimani A, Nousiainen P, Axelsson M, Mikulski M. Variable valve actuation (VVA) for next-generation marine and off-road engines: a comprehensive review for meeting future emissions legislation. Appl Energy 2026;406:127133. https://doi.org/10.1016/j.apenergy.2025.127133.

[20] Disassa HD, Ancha VR, Nallamothu RB, Zeru BA. Experimental study on the effect of speed and port-injected fuel blend ratio on a reactivity-control compression ignition (RCCI) engine performance. Energy Convers Manage: X 2023;20:100448. https://doi.org/10.1016/j.ecmx.2023.100448.

[21] Yahyaei SMJ, Gharehghani A, Andwari AM. Comprehensive numerical investigation of biodiesel/natural gas dual-fuel compression ignition engine with hydrogen and oxygen enrichment. Int J Hydrogen Energy 2025;98:254–65. https://doi.org/10.1016/j.ijhydene.2024.12.064.

[22] Moradi J, Gharehghani A, Aghahasani M. Application of machine learning to optimize the combustion characteristics of RCCI engine over wide load range. Fuel 2022;324:124494. https://doi.org/10.1016/j.fuel.2022.124494.

[23] L. Cao *et al.*, "Studying the Influence of Direct Injection on PCCI Combustion and Emissions at Engine Idle Condition Using Two Dimensional CFD and Stochastic Reactor Model," in *SAE World Congress & Exhibition*, SAE International, Apr. 2008. doi: https://doi.org/10.4271/2008-01-0021.

[24] Su H, Mosbach S, Kraft M, Bhave A, Kook S, Bae C. Two-stage fuel direct injection in a diesel fuelled HCCI engine. SAE Technical Papers 2007. https://doi.org/10.4271/2007-01-1880.

[25] V. De Bellis, E. Malfi, A. Lanotte, M. De Felice, L. Teodosio, and F. Bozza, "A Tabulated Chemistry Multi-Zone Combustion Model of HCCI Engines Supplied with Pure Fuel and Fuel Blends," *Energies (Basel).*, vol. 16, no. 1, 2023, doi: 10.3390/en16010265.

[26] S. M. Lashkarpour, R. Khoshbakhti Saray, and M. Najafi, "Multi-zone model for reactivity controlled compression ignition engine based on CFD approach," *Energy*, vol. 156, pp. 213–228, Aug. 2018, doi: 10.1016/j.energy.2018.05.084.

[27] Kodavasal J, et al. An accelerated multi-zone model for engine cycle simulation of homogeneous charge compression ignition combustion. Int J Engine Res 2013;14:416–33. https://doi.org/10.1177/1468087413482480.

[28] Egüz U, Maes NCJ, Leermakers CAJ, Somers LMT, De Goey LPH. Predicting auto-ignition characteristics of RCCI combustion using a multi-zone model. Int J Automot Technol 2013;14(5):693–9. https://doi.org/10.1007/s12239-013-0075-2.

[29] Eichmeier J, Reitz R, Rutland C. A zero-dimensional phenomenological model for RCCI combustion using reaction kinetics. SAE Int J Engines 2014;7:106–19. https://doi.org/10.4271/2014-01-1074.

[30] H. Hiroyasu and M. Arai, "Structures of Fuel Sprays in Diesel Engines," in *International Congress & Exposition*, SAE International, Feb. 1990. doi: https://doi.org/10.4271/900475.

[31] Mikulski M, Wierzbicki S, Piętak A. Zero-dimensional 2-phase combustion model in a dual-fuel compression ignition engine fed with gaseous fuel and a divided diesel fuel charge. Eksploatacja i Niezawodnosc - Maintenance and Reliability 2015;17:42–8. https://doi.org/10.17531/ein.2015.1.6.

[32] Bekdemir C, Baert R, Willems F, Somers LMT. Towards control-oriented modeling of natural gas-diesel RCCI combustion. SAE Technical Papers 2015;2015. https://doi.org/10.4271/2015-01-1745.

[33] Dahms RN. Understanding the breakdown of classic two-phase theory and spray atomization at engine-relevant conditions. Phys Fluids 2016;28(4):042108. https://doi.org/10.1063/1.4946000.

[34] A. Vasudev, A. Cafari, M. Axelsson, M. Mikulski, and J. Hyvonen, "Towards Next Generation Control-Oriented Thermo-Kinetic Model for Reactivity Controlled Compression Ignition Marine Engines," in *SAE Technical Papers*, SAE International, Aug. 2022. doi: 10.4271/2022-01-1033.

[35] A. Kakoee, A. Vasudev, B. Smulter, J. Hyvonen, and M. Mikulski, "A Predictive 1D Modeling Framework for Reactivity-Controlled Compression Ignition Engines, via a Chemistry-Based, Multizone Combustion Object," in *SAE Technical Papers*, SAE International, Aug. 2023. doi: 10.4271/2023-24-0001.

[36] M. Mikulski, T. Ovaska, R. Rabetino, M. Kangasjärvi, and A. Myllykangas, "Clean Propulsion Technologies: Securing Technological Dominance for the Finnish Marine and Off-Road Powertrain Sectors," *Energies (Basel).*, vol. 18, p. 1240, Mar. 2025, doi: 10.3390/en18051240.

[37] McNenly M. Integration strategies for efficient multizone chemical kinetics models. SAE Int J Fuels Lubr 2010;3:241–55. https://doi.org/10.4271/2010-01-0576.

[38] Zhou Y, Gainey B, Lawler B. An ultrafast multi-zone HCCI model with Autoignition, Global reaction and Interpolation (AGI) for achieving comparable accuracy to detailed chemical kinetics models. Combust Flame 2020;221:487–501. https://doi.org/10.1016/j.combustflame.2020.08.016.

[39] Fakhari AH, Salahi MM, Gharehghani A, Hunicz J, Mikulski M, Andwari AM. Novel chemical kinetic mechanism for CFD simulation of hydrogen-enriched natural gas/diesel RCCI combustion. Int J Hydrogen Energy 2025;105:1408–24. https://doi.org/10.1016/j.ijhydene.2025.01.451.

[40] Chang J, et al. New Heat transfer Correlation for an HCCI Engine Derived from Measurements of Instantaneous Surface Heat Flux. SAE Technical Papers 2004. https://doi.org/10.4271/2004-01-2996.

[41] Yao T, Pei Y, Zhong B-J, Som S, Lu T, Luo KH. A compact skeletal mechanism for n-dodecane with optimized semi-global low-temperature chemistry for diesel engine simulations. Fuel 2017;191:339–49.

[42] Behnoudfar P, Calo VM, Łoś M, Maczuga P, Paszyński M. A variational splitting of high-order linear multistep methods for heat transfer and advection–diffusion parabolic problems. J Comput Sci 2022;63:101807. https://doi.org/10.1016/j.jocs.2022.101807.

[43] A. Kakoee, J. Hunicz, and M. Mikulski, "Integrated 1D Simulation of Aftertreatment System and Chemistry-Based Multizone RCCI Combustion for Optimal Performance with Methane Oxidation Catalyst," *J. Mar. Sci. Eng.*, vol. 12, no. 4, Apr. 2024, doi: 10.3390/jmse12040594.

[44] Huang H, et al. Development of a new reduced diesel/natural gas mechanism for dual-fuel engine combustion and emission prediction. Fuel 2018;236:30–42. https://doi.org/10.1016/j.fuel.2018.08.161.

[45] G. H. Golub and C. F. Van Loan, *Matrix Computations*. in Johns Hopkins Studies in the Mathematical Sciences. Johns Hopkins University Press, 2013. [Online]. Available: https://books.google.fi/books?id=X5YfsuCWpxMC.